

Symmetry-preserved cost functions for variational quantum eigensolver

Hamzat Akande,^{1,2} Bruno Senjean,³ and Matthieu Saubanère^{1,*}

¹Université de Bordeaux, CNRS, LOMA, UMR 5798, F-33400 Talence, France

²ICTP-East African Institute for Fundamental Research, University of Rwanda, Kigali, Rwanda

³ICGM, Univ Montpellier, CNRS, ENSCM, Montpellier, France

Hybrid quantum-classical variational algorithms are considered ideal for noisy quantum computers, as they significantly reduce quantum circuit depth compared to fully quantum methods like quantum phase estimation. This reduction requires a classical variational optimization task. Ideally, circuits are shallow enough to avoid quantum noise, and the cost function is convex but not flat, enabling efficient optimization. However, quantum circuits based on unitary coupled cluster ansätze scale quartically with the number of qubits. Hardware-Efficient Ansätze (HEA) offer shallower circuits but suffer from optimization issues, including symmetry breaking. We propose encoding symmetry preservation directly into the cost function, enabling more efficient use of HEA. Our variational, iterative algorithm controls circuit depth and optimization challenges.

The many-body problem presents a major challenge in determining electronic ground-state energies using classical methods. Quantum computing offers a promising approach to addressing the exponential complexity of this problem [1–3]. However, current noisy intermediate-scale quantum (NISQ) devices face limitations such as short qubit coherence times and limited error correction, making quantum algorithms like phase estimation impractical [4, 5]. As a result, hybrid algorithms such as the variational quantum eigensolver (VQE) have been developed and successfully implemented on existing quantum hardware, offering a viable approach until fault-tolerant quantum computers become available [6–10].

The VQE algorithm optimizes a variational trial state to minimize the ground-state energy [6, 7]. This state preparation involves encoding the trial state in a quantum circuit using an ansatz, a unitary transformation applied to an initial state. Variational quantum ansätze can be broadly classified into two families: physically-motivated and hardware-efficient ansätze. The former, derived from classical physical approaches. A prominent example is the unitary coupled-cluster (UCC) ansatz, which underpins several related methods [6, 11–20]. These ansätze have desirable properties like symmetry-preserving and size extensivity but require deep circuits that are challenging to execute on current quantum hardware [21–23]. Adaptive algorithms such as ADAPT-VQE and the COMPASS approaches aim to reduce the number of excitation operators by selecting the most impactful ones, improving optimization and preventing overly deep circuits [24]. However, even with these advances [25–33], estimating ground-state energies for small molecules still requires circuits with tens of thousands of gates, exceeding current quantum device capabilities [35] and introducing measurement overhead as system sizes grow [24].

Hardware-efficient ansätze (HEA) use repeated layers of parametrized single-qubit rotations and entangling

gates, which are easy to implement on quantum processors. These methods have been effective for calculating the ground-state energies of small molecules [36, 37]. However, the use of HEA introduces scalability issues for larger systems, arising from (i) the lack of physico-chemical insight or symmetry constraints in the ansatz, and (ii) the presence of redundant variational parameters when many layers are considered, leading to global optimization issues and barren plateaus [38–42]. To address this, symmetry-preserving and symmetry-restoring algorithms have been developed, enabling low-depth circuits while maintaining physical symmetries [12, 21, 33, 43–47]. Additionally, several strategies have been proposed to handle challenging parameter optimization, such as using adaptive techniques [48], avoiding random initialization [49], using classical shadows [50], measuring compatible two-qubit local functions [51], or applying global minimization algorithms like sequential minimal optimization [52] or basin-hopping algorithms [53, 54].

In this contribution, we propose an alternative strategy that designs a cost function which preserves *de facto* the symmetry, regardless of the ansatz used to define the unitary transformation. An iterative procedure is introduced and allows to control the ratio between the circuit depth, the number of variational parameter and the number of measurements required to achieve the desired accuracy. As a proof of concept, we apply our flexible and versatile algorithm to the H₂ and H₄ molecular chains, targeting both the ground-state energy and the charge gap. Convergence properties in terms of circuit depth and number of iterations are also provided.

Let us consider the electronic Hamiltonian operator $\hat{\mathbf{H}}$ of a system for which the ground state is not degenerate. The Hamiltonian is expanded in the many-body Fock-space basis set $\{|\Phi_i\rangle\}$,

$$\hat{\mathbf{H}} = \sum_{ij} H_{ij} |\Phi_i\rangle \langle \Phi_j|, \quad (1)$$

where $\{|\Phi_i\rangle\}$ denote Slater determinants or configuration state functions, and we refer to $|\Phi_0\rangle$ as the Hartree–Fock (HF) Slater determinant. $\hat{\mathbf{H}}$ can be diagonalized using a

* matthieu.saubanere@cnrs.fr

unitary transformation matrix, $\bar{\mathbf{H}} = \mathbf{P}^\dagger \mathbf{H} \mathbf{P}$, where $\bar{H}_{ij} = E_i \delta_{ij}$ and E_i is the i^{th} eigenvalue sorted in ascending order. The eigenvectors are obtained as $|\Psi_i\rangle = \mathbf{P}|\Phi_i\rangle$, $|\Psi_0\rangle$ and E_0 thus correspond to the ground-state vector and energy, respectively. A standard approach to reach the lowest eigenvalue of $\hat{\mathbf{H}}$ on a quantum computer relies on the variational principle,

$$E_0 < E(\boldsymbol{\theta}^*) = \min_{\boldsymbol{\theta}} \langle \Phi_0 | \mathbf{P}^\dagger(\boldsymbol{\theta}) \hat{\mathbf{H}} \mathbf{P}(\boldsymbol{\theta}) | \Phi_0 \rangle, \quad (2)$$

where the unitary transformation $\mathbf{P}(\boldsymbol{\theta})$ depends on parameters $\boldsymbol{\theta}$ to be optimized, and $\boldsymbol{\theta}^*$ denotes the optimal parameters. At the saddle point, $|\Psi_0(\boldsymbol{\theta}^*)\rangle = \mathbf{P}(\boldsymbol{\theta}^*)|\Phi_0\rangle$, and if $\mathbf{P}(\boldsymbol{\theta}^*) = \mathbf{P}$, then $|\Psi(\boldsymbol{\theta}^*)\rangle = |\Psi_0\rangle$ and $E(\boldsymbol{\theta}^*) = E_0$.

Alternatively, we rewrite the variational principle in Eq. (2) in terms of the many-body ground-state density matrices defined as

$$\bar{\mathbf{\Gamma}} = \langle \Psi_0 | \hat{\mathbf{\Gamma}} | \Psi_0 \rangle, \quad \mathbf{\Gamma} = \langle \Psi_0 | \hat{\mathbf{\Gamma}} | \Psi_0 \rangle, \quad (3)$$

where $\hat{\mathbf{\Gamma}} = \sum_{ij} |\Psi_i\rangle \langle \Psi_j|$ and $\hat{\mathbf{\Gamma}} = \sum_{ij} |\Phi_i\rangle \langle \Phi_j|$ are the density matrix operators in the diagonal and many-body basis set representations, respectively. As depicted in Fig. 1(a), $\bar{\Gamma}_{ij} = \delta_{i0} \delta_{j0}$ for all i and j values. In this framework, the ground-state energy E_0 is computed as the following convolution,

$$E_0 = \text{tr}(\mathbf{\Gamma} \mathbf{H}) = \text{tr}(\bar{\mathbf{\Gamma}} \bar{\mathbf{H}}) = \bar{H}_{00}, \quad (4)$$

and the variational principle in Eq. (2) corresponds to

$$E_0 < E(\boldsymbol{\theta}^*) = \min_{\boldsymbol{\theta}} [\text{tr}(\bar{\mathbf{\Gamma}} \mathbf{P}^\dagger(\boldsymbol{\theta}) \mathbf{H} \mathbf{P}(\boldsymbol{\theta}))], \quad (5)$$

where tr denotes the trace and $E(\boldsymbol{\theta}^*) = E_0$ for $\mathbf{P}(\boldsymbol{\theta}^*) = \mathbf{P}$.

We introduce a third intermediate representation in which the first vector $|\Phi_0\rangle$ remains unchanged, and the density matrix

$$\tilde{\mathbf{\Gamma}} = \begin{bmatrix} \tilde{\mathbf{\Gamma}}^R & \mathbf{0} \\ \mathbf{0} & \mathbf{0} \end{bmatrix} \quad (6)$$

is block-diagonal. $\tilde{\mathbf{\Gamma}}^R$ is a 2×2 matrix that reads

$$\tilde{\mathbf{\Gamma}}^R = \begin{bmatrix} \Gamma_{00} & \tilde{\Gamma}_{10} \\ \tilde{\Gamma}_{01} & \tilde{\Gamma}_{11} \end{bmatrix} = \begin{bmatrix} \omega^2 & \sqrt{\omega^2(1-\omega^2)} \\ \sqrt{\omega^2(1-\omega^2)} & 1-\omega^2 \end{bmatrix}, \quad (7)$$

where $\omega^2 = |\langle \Psi_0 | \Phi_0 \rangle|^2$ represents the weight of $|\Phi_0\rangle$ in the ground state. This representation is called the Householder representation since, among all unitary transformations \mathbf{R} that provide the form of $\tilde{\mathbf{\Gamma}}$ in Eq. (6),

$$\tilde{\mathbf{\Gamma}} = \mathbf{R} \tilde{\mathbf{\Gamma}}^R \mathbf{R}, \quad (8)$$

with $|\Phi_0\rangle = \mathbf{R}|\Phi_0\rangle$, the Householder reflection ($\mathbf{R} = \mathbf{R}^\dagger$) is uniquely defined from the first column of $\mathbf{\Gamma}$. Note that this transformation has been recently used in the context of

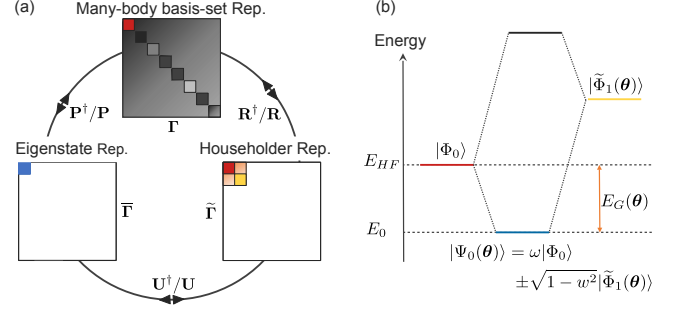


FIG. 1: (a) Schematic representation of the ground-state many-body density matrices $\mathbf{\Gamma}$, $\bar{\mathbf{\Gamma}}$, and $\tilde{\mathbf{\Gamma}}$ in the three different representations, namely the many-body basis set, eigenvector, and Householder representation. The unitary transformations \mathbf{P} , \mathbf{U} , and \mathbf{R} linking the three representations are displayed. (b) Schematic representation of the two-level decomposition of the ground state. We propose to optimize the gain energy E_G coming from the interaction between the *good-guess* $|\Phi_0\rangle$ and a variational vector $|\tilde{\Phi}_1(\boldsymbol{\theta})\rangle$.

embedding methods in electronic structure theory [55–58]. Using this transformation, the ground-state vector is decomposed as

$$|\Psi_0\rangle = \omega|\Phi_0\rangle + \nu\sqrt{1-\omega^2}\mathbf{R}|\Phi_1\rangle, \quad (9)$$

where $\nu = \pm 1$ is a relative phase factor, and the ground-state energy reads, in this new representation,

$$E_0 = \text{tr}(\tilde{\mathbf{\Gamma}} \tilde{\mathbf{H}}) = \text{tr}(\tilde{\mathbf{\Gamma}}^R \tilde{\mathbf{H}}^R), \quad (10)$$

where $\tilde{\mathbf{H}} = \mathbf{R} \mathbf{H} \mathbf{R}$ and

$$\tilde{\mathbf{H}}^R = \begin{bmatrix} H_{00} & \tilde{H}_{10} \\ \tilde{H}_{01} & \tilde{H}_{11} \end{bmatrix}. \quad (11)$$

It follows that the variational principle in Eq. (5) can be rewritten in the Householder representation as

$$E_0 < E(\boldsymbol{\theta}^*, \omega^*) = \min_{\omega, \boldsymbol{\theta}} [\text{tr}(\tilde{\mathbf{\Gamma}}^R(\omega) \tilde{\mathbf{H}}^R(\boldsymbol{\theta}))], \quad (12)$$

where $\boldsymbol{\theta}^*$ and ω^* are the minimizing parameters, and

$$\tilde{\mathbf{H}}^R(\boldsymbol{\theta}) = \begin{bmatrix} H_{00} & \tilde{H}_{10}(\boldsymbol{\theta}) \\ \tilde{H}_{01}(\boldsymbol{\theta}) & \tilde{H}_{11}(\boldsymbol{\theta}) \end{bmatrix}, \quad (13)$$

with $\tilde{\mathbf{H}}(\boldsymbol{\theta}) = \mathbf{R}^\dagger(\boldsymbol{\theta}) \mathbf{H} \mathbf{R}(\boldsymbol{\theta})$. By introducing the Householder representation, we have split the variational process into two sub-processes: 1) the optimization of the reflection $\mathbf{R}(\boldsymbol{\theta})$ to block-diagonalize $\mathbf{\Gamma}$ into $\tilde{\mathbf{\Gamma}}$, and 2) the optimization of the unitary $\mathbf{U}(\omega)$ to diagonalize $\tilde{\mathbf{H}}^R(\boldsymbol{\theta})$, i.e. $\mathbf{P} = \mathbf{R} \mathbf{U}$, see Fig. (1). Note that since $\tilde{\mathbf{\Gamma}}$ is idempotent, $\mathbf{U}(\omega)$ is only defined by a single parameter ω . Optimizing $\mathbf{R}(\boldsymbol{\theta})$ consists in finding the complementary vector $|\tilde{\Phi}_1(\boldsymbol{\theta})\rangle = \mathbf{R}(\boldsymbol{\theta})|\Phi_1\rangle$ of $|\Phi_0\rangle$ that composes the ground state, as shown in Eq. (9).

Let us make the strong assumption that $|\Phi_0\rangle$ is a *good-guess* for $|\Psi_0\rangle$, defined here through the condition $\omega^2 = |\langle\Phi_0|\Psi_0\rangle|^2 \geq 0.5$. In that case, instead of using the energy as a cost function to be minimized, we consider the so-called gain energy,

$$E_G(\boldsymbol{\theta}) = \frac{\Delta(\boldsymbol{\theta})}{2} \left[1 - \sqrt{1 + \frac{4\tilde{H}_{01}(\boldsymbol{\theta})\tilde{H}_{10}(\boldsymbol{\theta})}{\Delta(\boldsymbol{\theta})^2}} \right], \quad (14)$$

where $\Delta(\boldsymbol{\theta}) = |\tilde{H}_{11}(\boldsymbol{\theta}) - H_{00}|$. $E_G(\boldsymbol{\theta})$ is negative and corresponds to the energy stabilization resulting from the two-level system composed of $|\tilde{\Phi}_1(\boldsymbol{\theta})\rangle$ and $|\Phi_0\rangle$, as shown in Fig. 1(b). The ground-state energy E_0 is simply computed as the summation between the Hartree-Fock energy H_{00} and the gain energy,

$$E_0 = H_{00} + E_G(\boldsymbol{\theta}^*), \quad (15)$$

for the optimal parameter $\boldsymbol{\theta}^*$. Importantly, $E_G(\boldsymbol{\theta}) = 0$ if $|\tilde{\Phi}_1(\boldsymbol{\theta})\rangle$ and $|\Phi_0\rangle$ do not belong to the same symmetry-defined subspace of the Hamiltonian, i.e., if $\tilde{H}_{01}(\boldsymbol{\theta}) = \langle\Phi_0|\hat{H}|\tilde{\Phi}_1(\boldsymbol{\theta})\rangle = 0$. This property is expected to drastically simplify the energy landscape and ensure that for the optimal parameter $\boldsymbol{\theta}^*$ minimizing E_G , $|\tilde{\Phi}_1(\boldsymbol{\theta}^*)\rangle$ exhibits the same quantum numbers ($\langle N \rangle$, $\langle S^2 \rangle$, $\langle S_z \rangle$, for instance) as $|\Phi_0\rangle$, regardless of the ansatz used to construct $\mathbf{R}(\boldsymbol{\theta})$. Using $E_G(\boldsymbol{\theta})$ instead of the ground-state energy is then expected to leverage the use of HEA for VQE algorithms while preserving the symmetry of the system.

Practically speaking, even though recent progress has been made, constructing a reflection on a quantum computer is not straightforward, as it requires the use of multi-controlled NOT gates [59, 60]. However, the Householder transformation is one of many unitary transformations that block-diagonalize the density matrix while keeping $|\Phi_0\rangle$ unchanged. Consequently, rather than constraining the form of the unitary transformation to be a reflection, we use a unitary HEA to implement an ersatz $\mathbf{R}(\boldsymbol{\theta})$ to perform the block diagonalization. Following Re. [36] we choose the R_y CNOT ansatz as shown in Appendix A.

From a quantum circuit and measurement perspective, using E_G as the objective function requires additional measurements compared to standard VQE. Specifically, it necessitates measuring both $\tilde{H}_{11}(\boldsymbol{\theta}) = \langle\tilde{\Phi}_1(\boldsymbol{\theta})|\hat{H}|\tilde{\Phi}_1(\boldsymbol{\theta})\rangle$ and $|\tilde{H}_{01}(\boldsymbol{\theta})|^2 = |\langle\Phi_0|\hat{H}|\tilde{\Phi}_1(\boldsymbol{\theta})\rangle|^2$. The former is a standard projective measurement, while the latter has recently been shown to be efficiently measured without any ancilla qubits or the expensive application of Hadamard tests [61, 62].

Concerning optimization, to avoid constrained minimization to ensure $\mathbf{R}(\boldsymbol{\theta})|\Phi_0\rangle = |\Phi_0\rangle$, the cost function can be modified using a Gram-Schmidt process to directly encode the constraint, see Appendix B. However, an additional measurement of $\langle\Phi_0|\mathbf{R}(\boldsymbol{\theta})|\Phi_0\rangle$ is needed and can also be performed following [61, 62]. Altogether, each

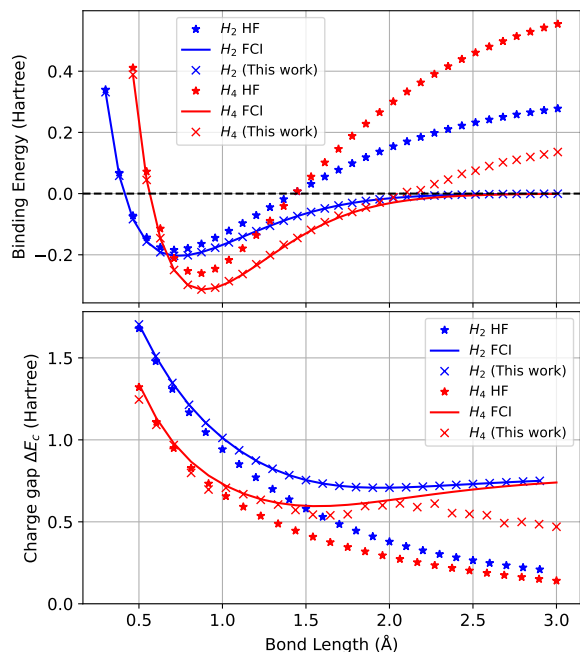


FIG. 2: Binding energy and charge gap as a function of the H-H inter-atomic distance in Å for H_2 and H_4 chains. We compare state vector simulation of our algorithm with Hartree-Fock mean field results and exact diagonalisation (FCI).

computation of the objective function requires at least the estimation of three quantities, whereas the energy only is needed in standard VQE. Note that, in contrast to standard VQE, a circuit representing the ground-state vector is never constructed on the quantum computer.

In Fig. 2, we show the binding energy and charge gap as a function of the interatomic distance for H_2 and H_4 chains. Results obtained by minimizing the cost function Eq. (14) with a HEA of depth n are compared to HF and full configuration interaction (FCI) data. The binding energy is computed as $E_B = E_0 - E_D$, where E_D is the dissociation energy computed at the FCI level at large H-H distance. The charge gap is calculated as $\Delta E_c = E_0(N_e + 1) + E_0(N_e - 1) - 2E_0(N_e)$, where $E_0(X)$ corresponds to the ground-state energy of the system with X electrons, and N_e is the number of electrons in the neutral system. At the mean-field level, ΔE_c corresponds to the energy gap between the highest occupied and the lowest unoccupied molecular orbitals, i.e., the HOMO-LUMO gap. For both the binding energy and charge gap, perfect agreement is reached between our results and FCI calculations, except for the H_4 chain with interatomic distances exceeding 2 Å. The accurate results for the charge gap demonstrates that using Eq. (14) as a cost function enforces the minimization to remain in the desired symmetry-defined subspace. Importantly, one would obtain $\Delta E_c = 0$ for all interatomic distances by using standard VQE with HEA. Indeed, in that case the optimization should end up in the same global minimum

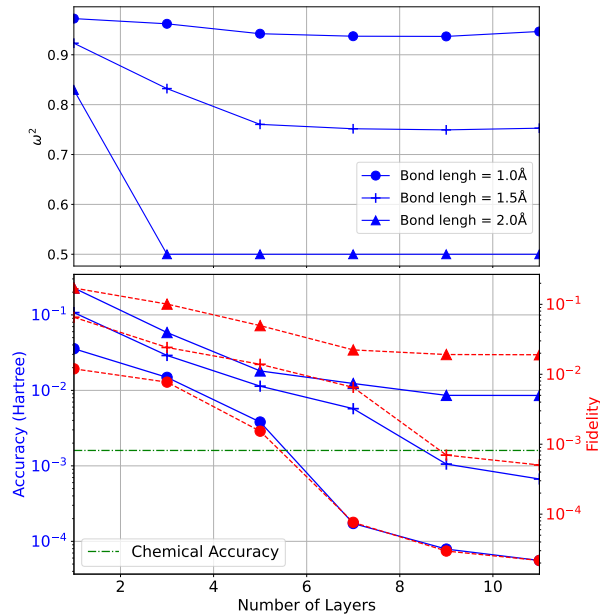


FIG. 3: Weight ω^2 (top), accuracy and fidelity (bottom) as a function of the number of layers for the H_4 chain with interatomic distances of 1.0, 1.5 and 2.0 Å.

regardless of the number of electrons in the system.

In Fig. 3, we show the convergence properties and more precisely, the accuracy, fidelity, and weight ω^2 as a function of the number of layers for the H_4 chains with interatomic distances of 1.0, 1.5, and 2.0 Å. For 1.0 and 1.5 Å, chemical accuracy of 1.6 mHartree is achieved at 7 and 9 layers, respectively. For 2.0 Å, after 9 layers, the energy and fidelity do not improve with additional layers. This behavior results from the violation of the *good-guess* assumption, illustrated here by the fact that ω^2 , obtained by diagonalizing the optimized $\tilde{\mathbf{H}}^R(\theta^*)$, saturates at a value of 1/2 after only 3 layers. Indeed, when the initial state is a *bad-guess* (i.e. $|\langle \Phi_0 | \Psi_0 \rangle|^2 < 0.5$), minimizing $E_G(\theta)$ with the condition $H_{00} < \tilde{H}_{11}(\theta)$ favors maximal interaction between $|\Phi_0\rangle$ and $|\tilde{\Phi}_1(\theta)\rangle$, thus leading to $\omega^2 = 1/2$ after optimization [see Eq. (9)]. The energy associated to $|\Psi_0(\theta^*)\rangle$ is nevertheless reduced compared to the initial energy of $|\Phi_0\rangle$, making $|\Psi_0(\theta^*)\rangle$ a better *good-guess* than $|\Phi_0\rangle$. Consequently, we propose an iterative algorithm for which the loop condition requires that the ground state $|\Psi_0^{(i)}(\theta^{(i)*})\rangle$ of the two-level system obtained at the end of iteration i becomes the *good-guess* $|\Phi_0^{(i+1)}\rangle$ of the next iteration. The iteration algorithm can be divided into the following steps, starting at iteration $i = 1$:

1. *Define the good-guess vector as $|\Psi_0^{(i-1)}\rangle$.* Note that we have $|\Psi_0^{(i=0)}\rangle = |\tilde{\Phi}_1^{(i=0)}\rangle = |\Phi_0\rangle$ before doing any iteration.
2. *Optimize the reflection $\mathbf{R}(\theta^{(i)})$.* We opti-

mize the gain energy $E_G^{(i)}(\theta^{(i)})$ under the orthogonality constraint $\langle \tilde{\Phi}_1^{(i)}(\theta^{(i)}) | \Psi_0^{(i-1)} \rangle = 0$, where $|\tilde{\Phi}_1^{(i)}(\theta^{(i)})\rangle = R(\theta^{(i)})|\Phi_i\rangle$. This requires measuring every $\langle \tilde{\Phi}_1^{(j)}(\theta^{(j)*}) | \tilde{\Phi}_1(\theta^{(i)}) \rangle$ and $\langle \tilde{\Phi}_1^{(j)}(\theta^{(j)*}) | \hat{\mathbf{H}} | \tilde{\Phi}_1(\theta^{(i)}) \rangle$ for $j \leq i$. See Eq. (14), main text and Appendix B for more details. The minimizing parameters are denoted by $\theta^{(i)*}$.

3. *Update good-guess.* We diagonalize $\tilde{\mathbf{H}}^R(\theta^{(i)*})$, expanded in the subspace spanned by $|\Psi_0^{(i-1)}\rangle$ and $|\tilde{\Phi}_1^{(i)}(\theta^{(i)*})\rangle$, to obtain the optimal $\omega^{(i)*}$ [see Eq. (9)]. This leads to

$$|\Psi_0^{(i)}\rangle = \omega^{(i)*} |\Psi_0^{(i-1)}\rangle \pm \sqrt{1 - (\omega^{(i)*})^2} |\tilde{\Phi}_1^{(i)}(\theta^{(i)*})\rangle$$

4. *Check convergence.* If $(\omega^{(i)*})^2 \rightarrow 1$ then the process is converged. Otherwise, one can start again at step 1 with $i = i + 1$.

Note that step 3 of the algorithm could be revised in the same spirit as quantum subspace expansion (QSE) approaches. Indeed, we could diagonalize the $(i \times i)$ Hamiltonian matrix instead of the (2×2) $\tilde{\mathbf{H}}^R(\theta^{(i)*})$ matrix, as all $\langle \tilde{\Phi}_1^{(j)}(\theta^{(j)*}) | \hat{\mathbf{H}} | \tilde{\Phi}_1^{(i)}(\theta^{(i)*}) \rangle$ elements have already been measured. In other words, the set of $\{|\Phi_0\rangle, |\tilde{\Phi}_1^{(i)}(\theta^{(i)})\rangle\}_i$ constitutes a reduced basis in which the Hamiltonian is expanded [61–65]. This procedure is depicted in the top panel of Fig. 4.

In the middle and bottom panel of Fig. 4, the convergence of the iterative algorithm is shown as a function of the iteration number for the H_4 chain with interatomic distances of 1 and 2 Å, respectively. Different circuit depths, ranging from 1 to 9 layers, have been considered. The error is shown to decrease rapidly and systematically regardless of the circuit depth. Importantly, achieving chemical accuracy with a single layer requires approximately 10 (respectively 5) iterations for 8 variational parameters optimized at each step, compared to a single optimization involving 72 parameters in a 9-layer circuit at 2 Å (respectively 1 Å). This strongly suggests that our iterative approach can help to bypass optimization issues, as one can use much shallower circuits with much less parameters to optimize, at the expense of more iterations.

Altogether, we propose an iterative and variational approach to compute the ground-state energy in a given symmetry-imposed subspace of the electronic Hamiltonian. The symmetries are encoded in a *good-guess* initial state and preserved throughout the minimization by using the gain energy E_G as the cost function, regardless of the unitary ansatz that is considered. Besides, the iterative algorithm allows to control the circuit depth and the number of parameters to optimize simultaneously, thereby reducing noise and potentially addressing optimization issues.

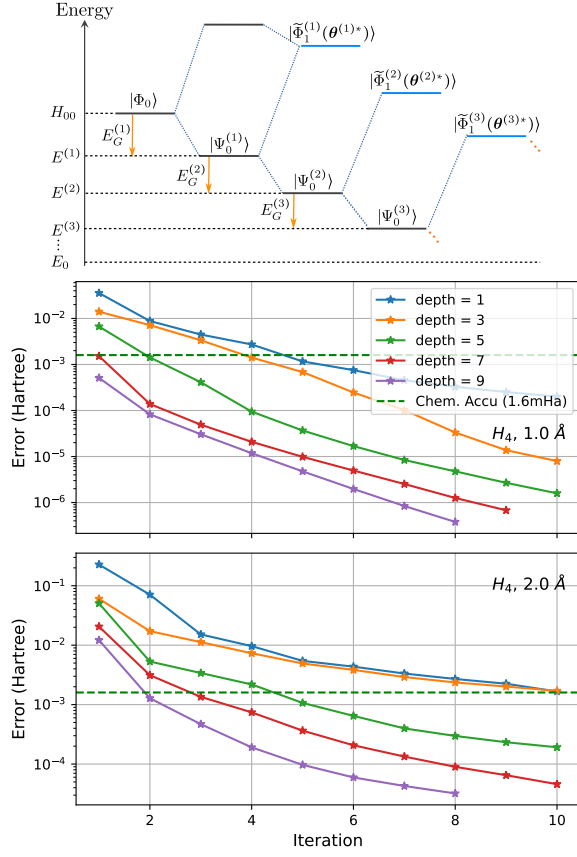


FIG. 4: Schematic depiction of the iterative algorithm (top panel). Only the states $\{|\tilde{\Phi}_1^{(i)}(\theta^{(i)})\rangle\}$ in blue are optimized on a quantum computer to minimize the gain energy $E_G^{(i)}(\theta^{(i)})$. Error as a function of the number of iteration for the H_4 chain with interatomic distances of 1 (middle panel) and 2 Å (bottom panel). Results are shown for different circuit depths corresponding to the number of layers in the HEA.

ACKNOWLEDGMENTS

HA is grateful to the Hubert Curien program (CAMPUS FRANCE) for the support as well as the Abdus Salam ICTP for the HPC facilities.

AUTHORS CONTRIBUTION

Algorithm implementation and data acquisition: H.A. (lead) and M.S. (support); Concept and methodology: M.S. (lead) and B.S. (support); Supervision and project management: MS; Writing original draft: M.S (lead) and B.S. (support). All authors edited and commented on the manuscript.

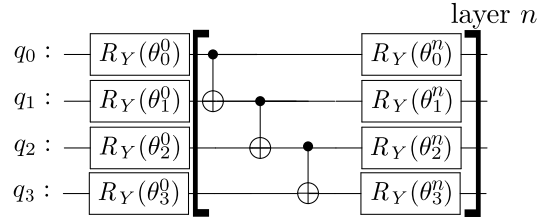


FIG. 5: Schematic representation of the HEA used in this work. The circuit inside the square brackets is repeated n times for n layers.

Appendix A: Hardware efficient ansatz:

We show in Fig. (5) the schematic picture of the R_y CNOT Hardware-Efficient Ansatz, see [36]. The Ansatz comprises a first layer of $R_y(\theta)$ gates on each qubit, followed by n layers containing a chain of two-qubit entangling gates (using a linear entanglement strategy) and one $R_y(\theta)$ rotation gate per qubit, see Fig. 5. The number of variational parameters is equal to $n(N_{\text{qubit}} + 1)$ and the number of CNOT to $n(N_{\text{qubit}} - 1)$.

Appendix B: Constrained cost function

To avoid a constrained minimization, one can directly set up the constrain $\mathbf{R}(\theta)|\Phi_0\rangle = |\Phi_0\rangle$ in the cost function. Starting from the constrain to fulfill,

$$\mathbf{R}(\theta)|\Phi_0\rangle = |\Phi_0\rangle, \quad (\text{B1})$$

we multiply on the left by $\langle\Phi_1|\mathbf{R}^\dagger(\theta)$ such that

$$\langle\Phi_1|\mathbf{R}^\dagger(\theta)\mathbf{R}(\theta)|\Phi_0\rangle = \langle\Phi_1|\mathbf{R}^\dagger(\theta)|\Phi_0\rangle, \quad (\text{B2})$$

which leads to, using $\mathbf{R}^\dagger\mathbf{R} = \mathbb{1}$ for the Householder transformation,

$$\langle\Phi_1|\Phi_0\rangle = \langle\tilde{\Phi}_1(\theta)|\Phi_0\rangle. \quad (\text{B3})$$

As the basis set is orthogonal, we end up with $\langle\tilde{\Phi}_1(\theta)|\Phi_0\rangle = 0$. We can then use a Gram-Schmidt orthonormalization process to constrain $|\tilde{\Phi}_1(\theta)\rangle$ to be orthonormal to $|\Phi_0\rangle$ as follows,

$$|\tilde{\Phi}_1^\perp(\theta)\rangle = \vartheta \left(z|\tilde{\Phi}_1(\theta)\rangle - \sqrt{1-z^2}|\Phi_0\rangle \right), \quad (\text{B4})$$

with $\langle\Phi_0|\tilde{\Phi}_1(\theta)\rangle = \vartheta|S|$, $\vartheta = \pm 1$ and $|S|$ are the sign and amplitude of the overlap, and $z = 1/\sqrt{1+S^2}$. The reduced Hamiltonian of the normalized two-level system from which the cost function is computed becomes

$$\tilde{\mathbf{H}}^{R\perp}(\theta) = H_{00}\mathbb{1} + \begin{bmatrix} 0 & \tilde{H}_{10}^\perp(\theta) \\ \tilde{H}_{01}^\perp(\theta) & \Delta^\perp(\theta) \end{bmatrix} \quad (\text{B5})$$

with $\tilde{H}_{10}^\perp(\theta) = \langle\Phi_0|\tilde{\mathbf{H}}|\tilde{\Phi}_1^\perp(\theta)\rangle$, $\tilde{H}_{11}^\perp(\theta) = \langle\tilde{\Phi}_1^\perp(\theta)|\tilde{\mathbf{H}}|\tilde{\Phi}_1^\perp(\theta)\rangle$, and $\Delta^\perp(\theta) = |\tilde{H}_{11}^\perp(\theta) - H_{00}|$. Note

that $|\tilde{\Phi}_1^+(\boldsymbol{\theta})\rangle$ is not prepared on the quantum circuit. According to Eq. (B4), only the overlap S has to be measured, so that all the matrix elements of Eq. (B5) can be determined on the classical computer. Turning to the iterative procedure described in the main text, the *good-guess* is replaced at each new iteration i by the

ground state $|\Psi_0^{(i-1)}\rangle$ of the two-level system built in the $(i-1)$ th iteration. Hence, the overlap $\langle\Psi_0^{(i-1)}|\tilde{\Phi}_1^{(i)}(\boldsymbol{\theta}^{(i)})\rangle$ has to be measured, which reduces to measure the overlap between $|\tilde{\Phi}_1^{(i)}(\boldsymbol{\theta}^{(i)})\rangle$ and the states involved in the preparation of $|\Psi_0^{(i-1)}\rangle$, i.e. $|\Phi_0\rangle$ and all $\{|\tilde{\Phi}_1^{(j)}(\boldsymbol{\theta}^{(j)*})\rangle\}$ with $j < i$.

- ¹ A. Aspuru-Guzik, A. D. Dutoi, P. J. Love, and M. Head-Gordon, Simulated Quantum Computation of Molecular Energies, *Science* **309**, 1704 (2005).
- ² B. Bauer, S. Bravyi, M. Motta, and G. K.-L. Chan, Quantum Algorithms for Quantum Chemistry and Quantum Materials Science, *Chem. Rev.* **120**, 12685 (2020).
- ³ S. McArdle, S. Endo, A. Aspuru-Guzik, S. C. Benjamin, and X. Yuan, Quantum computational chemistry, *Rev. Mod. Phys.* **92**, 015003 (2020).
- ⁴ K. Bharti, A. Cervera-Lierta, T. H. Kyaw, T. Haug, S. Alperin-Lea, A. Anand, M. Degroote, H. Heimonen, J. S. Kottmann, T. Menke, W.-K. Mok, S. Sim, L.-C. Kwek, and A. Aspuru-Guzik, Noisy intermediate-scale quantum algorithms, *Rev. Mod. Phys.* **94**, 015004 (2022).
- ⁵ P. J. J. O'Malley, R. Babbush, I. D. Kivlichan, J. Romero, J. R. McClean, R. Barends, J. Kelly, P. Roushan, A. Tranter, N. Ding, B. Campbell, Y. Chen, Z. Chen, B. Chiaro, A. Dunsworth, A. G. Fowler, E. Jeffrey, E. Lucero, A. Megrant, J. Y. Mutus, M. Neeley, C. Neill, C. Quintana, D. Sank, A. Vainsencher, J. Wenner, T. C. White, P. V. Coveney, P. J. Love, H. Neven, A. Aspuru-Guzik, and J. M. Martinis, Scalable Quantum Simulation of Molecular Energies, *Phys. Rev. X* **6**, 031007 (2016).
- ⁶ A. Peruzzo, J. McClean, P. Shadbolt, M.-H. Yung, X.-Q. Zhou, P. J. Love, A. Aspuru-Guzik, and J. L. O'Brien, A variational eigenvalue solver on a photonic quantum processor, *Nat Commun* **5**, 4213 (2014).
- ⁷ J. R. McClean, J. Romero, R. Babbush, and A. Aspuru-Guzik, The theory of variational hybrid quantum-classical algorithms, *New J. Phys.* **18**, 023023 (2016).
- ⁸ C. Hempel, C. Maier, J. Romero, J. McClean, T. Monz, H. Shen, P. Jurcevic, B. P. Lanyon, P. Love, R. Babbush, A. Aspuru-Guzik, R. Blatt, and C. F. Roos, Quantum Chemistry Calculations on a Trapped-Ion Quantum Simulator, *Phys. Rev. X* **8**, 031022 (2018).
- ⁹ D. A. Fedorov, B. Peng, N. Govind, and Y. Alexeev, VQE method: A short survey and recent developments, *Materials Theory* **6**, 2 (2022).
- ¹⁰ J. Tilly, H. Chen, S. Cao, D. Picozzi, K. Setia, Y. Li, E. Grant, L. Wossnig, I. Rungger, G. H. Booth, and J. Tennyson, The Variational Quantum Eigensolver: A review of methods and best practices, *Physics Reports* **986**, 1 (2022).
- ¹¹ M.-H. Yung, J. Casanova, A. Mezzacapo, J. McClean, L. Lamata, A. Aspuru-Guzik, and E. Solano, From transistor to trapped-ion computers for quantum chemistry, *Sci Rep* **4**, 3589 (2014).
- ¹² P. K. Barkoutsos, J. F. Gonthier, I. Sokolov, N. Moll, G. Salis, A. Fuhrer, M. Ganzhorn, D. J. Egger, M. Troyer, A. Mezzacapo, S. Filipp, and I. Tavernelli, Quantum algorithms for electronic structure calculations: Particle-hole Hamiltonian and optimized wave-function expansions, *Phys. Rev. A* **98**, 022322 (2018).
- ¹³ J. Romero, R. Babbush, J. R. McClean, C. Hempel, P. J. Love, and A. Aspuru-Guzik, Strategies for quantum computing molecular energies using the unitary coupled cluster ansatz, *Quantum Sci. Technol.* **4**, 014008 (2018).
- ¹⁴ J. Lee, W. J. Huggins, M. Head-Gordon, and K. B. Whaley, Generalized unitary coupled cluster wave functions for quantum computation, *J. Chem. Theory Comput.* **15**, 311 (2018).
- ¹⁵ F. A. Evangelista, G. K. Chan, and G. E. Scuseria, Exact parameterization of fermionic wave functions via unitary coupled cluster theory, *J. Chem. Phys.* **151** (2019).
- ¹⁶ I. O. Sokolov, P. K. Barkoutsos, P. J. Ollitrault, D. Greenberg, J. Rice, M. Pistoia, and I. Tavernelli, Quantum orbital-optimized unitary coupled cluster methods in the strongly correlated regime: Can quantum algorithms outperform their classical equivalents?, *J. Chem. Theory Comput.* **152**, 124107 (2020).
- ¹⁷ A. Khamoshi, G. P. Chen, F. A. Evangelista, and G. E. Scuseria, Agp-based unitary coupled cluster theory for quantum computers, *Quantum Sci. Technol.* **8**, 015006 (2022).
- ¹⁸ S. E. Smart and D. A. Mazziotti, Quantum Solver of Contracted Eigenvalue Equations for Scalable Molecular Simulations on Quantum Computing Devices, *Phys. Rev. Lett.* **126**, 070504 (2021).
- ¹⁹ Q. Marécat, B. Senjean, and M. Saubanière, Recursive relations and quantum eigensolver algorithms within modified Schrieffer-Wolff transformations for the Hubbard dimer, *Phys. Rev. B* **107**, 155110 (2023).
- ²⁰ D. Materia, L. Ratini, C. Angeli, and L. Guidoni, Quantum Information Driven Ansatz (QIDA): Shallow-Depth Empirical Quantum Circuits from Quantum Chemistry, *J. Phys. Chem. A* **10.1021/acs.jpca.4c03756** (2024).
- ²¹ B. O'Gorman, W. J. Huggins, E. G. Rieffel, and K. B. Whaley, Generalized swap networks for near-term quantum computing (2019), [arxiv:1905.05118](https://arxiv.org/abs/1905.05118) [physics, physics:quant-ph].
- ²² H. R. Grimsley, D. Claudino, S. E. Economou, E. Barnes, and N. J. Mayhall, Is the Trotterized UCCSD Ansatz Chemically Well-Defined?, *J. Chem. Theory Comput.* **16**, 1 (2020).
- ²³ M. Motta, E. Ye, J. R. McClean, Z. Li, A. J. Minnich, R. Babbush, and G. K.-L. Chan, Low rank representations for quantum simulation of electronic structure, *npj Quantum Inf* **7**, 1 (2021).
- ²⁴ H. R. Grimsley, S. E. Economou, E. Barnes, and N. J. Mayhall, An adaptive variational algorithm for exact molecular simulations on a quantum computer, *Nat Commun* **10**, 3007 (2019).
- ²⁵ J. Liu, L. Wan, Z. Li, and J. Yang, Simulating Periodic Systems on a Quantum Computer Using Molecular Orbitals, *J. Chem. Theory Comput.* **16**, 6904 (2020).

- ²⁶ C. Feniou, M. Hassan, D. Traoré, E. Giner, Y. Maday, and J.-P. Piquemal, Overlap-ADAPT-VQE: Practical quantum chemistry on quantum computers via overlap-guided compact Ansätze, *Commun Phys* **6**, 1 (2023).
- ²⁷ H. G. A. Burton, D. Marti-Dafcik, D. P. Tew, and D. J. Wales, Exact electronic states with shallow quantum circuits from global optimisation, *npj Quantum Inf* **9**, 1 (2023).
- ²⁸ N. Vaquero-Sabater, A. Carreras, R. Orús, N. J. Mayhall, and D. Casanova, Physically Motivated Improvements of Variational Quantum Eigensolvers, *J. Chem. Theory Comput.* **20**, 5133 (2024).
- ²⁹ Z. Sun, J. Liu, Z. Li, and J. Yang, *Circuit-Efficient Qubit-Excitation-based Variational Quantum Eigensolver* (2024), arxiv:2406.11699 [quant-ph].
- ³⁰ P. G. Anastasiou, Y. Chen, N. J. Mayhall, E. Barnes, and S. E. Economou, Tetris-adapt-vqe: Adaptive algorithm that yields shallower, denser circuit ansätze, *Phys. Rev. Res.* **6**, 013254 (2024).
- ³¹ C. Feniou, O. Adjoua, B. Claudon, J. Zylberman, E. Giner, and J.-P. Piquemal, Sparse Quantum State Preparation for Strongly Correlated Systems, *J. Phys. Chem. Lett.* **15**, 3197 (2024).
- ³² J. Liu, Z. Li, and J. Yang, Perturbative variational quantum algorithms for material simulations, *Electron. Struct.* **6**, 015007 (2024).
- ³³ H. G. A. Burton, Accurate and gate-efficient quantum ansätze for electronic states without adaptive optimization, *Phys. Rev. Res.* **6**, 023300 (2024).
- ³⁴ M. Ramôa, P. G. Anastasiou, L. P. Santos, N. J. Mayhall, E. Barnes, and S. E. Economou, *Reducing the Resources Required by ADAPT-VQE Using Coupled Exchange Operators and Improved Subroutines* (2024), arxiv:2407.08696.
- ³⁵ M.-A. Filip, N. Fitzpatrick, D. Muñoz Ramo, and A. J. W. Thom, Reducing unitary coupled cluster circuit depth by classical stochastic amplitude prescreening, *Phys. Rev. Res.* **4**, 023243 (2022).
- ³⁶ A. Kandala, A. Mezzacapo, K. Temme, M. Takita, M. Brink, J. M. Chow, and J. M. Gambetta, Hardware-efficient variational quantum eigensolver for small molecules and quantum magnets, *Nature* **549**, 242 (2017).
- ³⁷ M. Ganzhorn, D. Egger, P. Barkoutsos, P. Ollitrault, G. Salis, N. Moll, M. Roth, A. Fuhrer, P. Mueller, S. Wöerner, I. Tavernelli, and S. Filipp, Gate-Efficient Simulation of Molecular Eigenstates on a Quantum Computer, *Phys. Rev. Appl.* **11**, 044092 (2019).
- ³⁸ J. R. McClean, S. Boixo, V. N. Smelyanskiy, R. Babbush, and H. Neven, Barren plateaus in quantum neural network training landscapes, *Nat Commun* **9**, 4812 (2018).
- ³⁹ L. Bittel and M. Kliesch, Training Variational Quantum Algorithms Is NP-Hard, *Phys. Rev. Lett.* **127**, 120502 (2021).
- ⁴⁰ R. D’Cunha, T. D. Crawford, M. Motta, and J. E. Rice, Challenges in the Use of Quantum Computing Hardware-Efficient Ansätze in Electronic Structure Theory, *J. Phys. Chem. A* **127**, 3437 (2023).
- ⁴¹ M. Larocca, S. Thanasilp, S. Wang, K. Sharma, J. Biamente, P. J. Coles, L. Cincio, J. R. McClean, Z. Holmes, and M. Cerezo, A Review of Barren Plateaus in Variational Quantum Computing (2024), arxiv:2405.00781 [quant-ph, stat].
- ⁴² L. Leone, S. F. E. Oliviero, L. Cincio, and M. Cerezo, On the practical usefulness of the Hardware Efficient Ansatz, *Quantum* **8**, 1395 (2024).
- ⁴³ B. T. Gard, L. Zhu, G. S. Barron, N. J. Mayhall, S. E. Economou, and E. Barnes, Efficient symmetry-preserving state preparation circuits for the variational quantum eigensolver algorithm, *npj Quantum Inf* **6**, 1 (2020).
- ⁴⁴ K. Seki, T. Shirakawa, and S. Yunoki, Symmetry-adapted variational quantum eigensolver, *Phys. Rev. A* **101**, 052340 (2020).
- ⁴⁵ G.-L. R. Anselmetti, D. Wierichs, C. Gogolin, and R. M. Parrish, Local, expressive, quantum-number-preserving VQE ansätze for fermionic systems, *New J. Phys.* **23**, 113010 (2021).
- ⁴⁶ D. Lacroix, E. A. Ruiz Guzman, and P. Siwach, Symmetry breaking/symmetry preserving circuits and symmetry restoration on quantum computers, *Eur. Phys. J. A* **59**, 3 (2023).
- ⁴⁷ E. A. Ruiz Guzman and D. Lacroix, Restoring symmetries in quantum computing using Classical Shadows, *Eur. Phys. J. A* **60**, 112 (2024).
- ⁴⁸ I. G. Ryabinkin, T.-C. Yen, S. N. Genin, and A. F. Izmaylov, Qubit Coupled Cluster Method: A Systematic Approach to Quantum Chemistry on a Quantum Computer, *J. Chem. Theory Comput.* **14**, 6317 (2018).
- ⁴⁹ E. Grant, L. Wossnig, M. Ostaszewski, and M. Benedetti, An initialization strategy for addressing barren plateaus in parametrized quantum circuits, *Quantum* **3**, 214 (2019).
- ⁵⁰ S. H. Sack, R. A. Medina, A. A. Michailidis, R. Kueng, and M. Serbyn, Avoiding Barren Plateaus Using Classical Shadows, *PRX Quantum* **3**, 020365 (2022).
- ⁵¹ L. Zambrano, A. D. Muñoz-Moller, M. Muñoz, L. Pereira, and A. Delgado, Avoiding barren plateaus in the variational determination of geometric entanglement, *Quantum Sci. Technol.* **9**, 025016 (2024).
- ⁵² K. M. Nakanishi, K. Fujii, and S. Todo, Sequential minimal optimization for quantum-classical hybrid algorithms, *Phys. Rev. Res.* **2**, 043158 (2020).
- ⁵³ A. M. Alvertis, A. Khan, T. Iadecola, P. P. Orth, and N. Tubman, *Classical Benchmarks for Variational Quantum Eigensolver Simulations of the Hubbard Model* (2024), arxiv:2408.00836 [cond-mat, physics:quant-ph].
- ⁵⁴ B. Choy and D. J. Wales, Molecular Energy Landscapes of Hardware-Efficient Ansätze in Quantum Computing, *J. Chem. Theory Comput.* **19**, 1197 (2023).
- ⁵⁵ S. Sekaran, M. Tsuchiizu, M. Saubanère, and E. Fromager, Householder transformed density matrix functional embedding theory, *Phys. Rev. B* **104**, 10.1103/PhysRevB.104.035121 (2021).
- ⁵⁶ S. Yalouz, S. Sekaran, E. Fromager, and M. Saubanère, Quantum embedding of multi-orbital fragments using the block-Householder transformation, *The Journal of Chemical Physics* **157**, 214112 (2022).
- ⁵⁷ Q. Marécat, B. Lasorne, E. Fromager, and M. Saubanère, Unitary transformations within density matrix embedding approaches: A perspective on the self-consistent scheme for electronic structure calculation, *Phys. Rev. B* **108**, 155119 (2023).
- ⁵⁸ Q. Marécat and M. Saubanère, A Versatile Unitary Transformation Framework for an Optimal Bath Construction in Density-Matrix Based Quantum Embedding Approaches, *Computation* **11**, 203 (2023).
- ⁵⁹ F. Orts, G. Ortega, and E. M. Garzón, Studying the Cost of n-qubit Toffoli Gates, in *Computational Science – ICCS 2022*, edited by D. Groen, C. de Mulatier, M. Paszynski, V. V. Krzhizhanovskaya,

- J. J. Dongarra, and P. M. A. Sloot (Springer International Publishing, Cham, 2022) pp. 122–128.
- ⁶⁰ B. Claudon, J. Zylberman, C. Feniou, F. Debbasch, A. Peruzzo, and J.-P. Piquemal, Polylogarithmic-depth controlled-NOT gates without ancilla qubits, *Nat Commun* **15**, 5886 (2024).
- ⁶¹ C. L. Cortes and S. K. Gray, Quantum Krylov subspace algorithms for ground- and excited-state energy estimation, *Phys. Rev. A* **105**, 022417 (2022).
- ⁶² M. Motta, W. Kirby, I. Liepuoniute, K. J. Sung, J. Cohn, A. Mezzacapo, K. Klymko, N. Nguyen, N. Yoshioka, and J. E. Rice, Subspace methods for electronic structure simulations on quantum computers, *Electron. Struct.* **6**, 013001 (2024).
- ⁶³ J. R. McClean, M. E. Kimchi-Schwartz, J. Carter, and W. A. de Jong, Hybrid quantum-classical hierarchy for mitigation of decoherence and determination of excited states, *Phys. Rev. A* **95**, 042308 (2017).
- ⁶⁴ N. H. Stair, R. Huang, and F. A. Evangelista, A Multireference Quantum Krylov Algorithm for Strongly Correlated Electrons, *J. Chem. Theory Comput.* **16**, 2236 (2020).
- ⁶⁵ N. Yoshioka, H. Hakoshima, Y. Matsuzaki, Y. Tokunaga, Y. Suzuki, and S. Endo, Generalized Quantum Subspace Expansion, *Phys. Rev. Lett.* **129**, 020502 (2022).